Macromolecules

Article

pubs.acs.org/Macromolecules

Instabilities of PS/PMMA Bilayer Patterns with a Corrugated Surface and Interface

Zheng Zhang, Dae Up Ahn, and Yifu Ding*

Department of Mechanical Engineering, University of Colorado, Boulder, Colorado 80309-0427, United States

Supporting Information

ABSTRACT: We study the patterns spontaneously formed by bilayer polymer films upon annealing. Specifically, polystyrene (PS) films were spin-cast on topographically patterned poly(methyl methacrylate) (PMMA) substrates and subsequently annealed at temperatures above the glass transition temperature of both polymers. The influence of the molecular weight and the volume of PS on the morphological evolution of the corrugated liquid−liquid interface was examined. When the PS formed isolated stripes both on the mesas and within the trenches of the PMMA pattern, capillary instability was observed for these nonaxisymmetric PS threads. The kinetics of the capillary breakup depended on the thread-to-matrix viscosity ratio, and was dictated by the more viscous component. In contrast, the characteristic wavelength of the breakup only slightly depended on some viscosity ratio, and reached a minimum at the viscosity ratio around 1. When the PS was thick enough to form a continuous layer, the instability of the film further depended on the molecular weight of the PS. For a molecular weight of 13 kg/mol, the PS dewetted from PMMA via a random nucleation and growth mechanism. However, for a molecular weight of 2000 kg/mol, localized nucleation on top of the PMMA mesas led to a mesh-like PS morphology, which eventually broke up due to capillary instability. Therefore, by controlling the molecular weight and the spin-cast volume of the top layer, the kinetics of morphological evolution and the resulting patterns can be controlled.

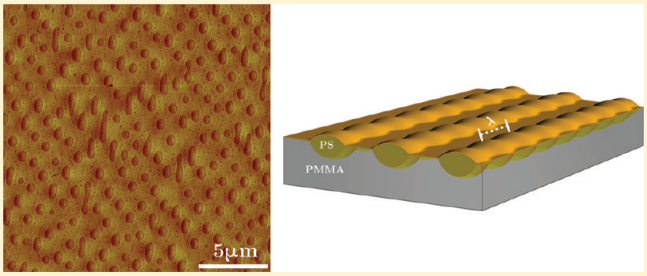

1. INTRODUCTION

Polymers, in thin films or nanostructured patterns, are subject to a range of surface and interfacial interactions. Understanding the characteristics of these interactions and the resulting instabilities is vital for achieving robust polymeric patterns and structures, especially during fabrication processes. The extent of these instabilities can be modulated by viscous and elastic effects. Understanding of these effects promises to create unique complex structures which are hard to approach with top-down lithographic methods.

Capillary fluctuations are ubiquitous at viscous polymer surfaces and interfaces. These fluctuations can lead to spontaneous rupture or dewetting of an ultrathin (<100 nm) polymer film on a nonwettable substrate, through a mechanism termed spinodal dewetting.[1] Thicker films are more resistant to these fluctuations. The fluctuations can be dramatically amplified under thermal[2] or electric[3,4] fields, which can rupture a normally stable film. In the absence of external fields, a thick polymer film can dewet from nonwettable substrates alternatively via a nucleation and growth mechanism.[5−7] Studies have shown that both types of dewetting can be guided or directed using topographically[8,9] or chemically[10,11] patterned substrates.

For polymer structures with large length-to-cross-section ratios, such as fibers, the capillary fluctuations along the axial direction can lead to rupture of the continuous structures. For a cylindrical liquid thread embedded within a viscous matrix, the characteristics of the capillary breakup, including both the wavelength and kinetics, are well captured by Tomotika's classical theory.[12] Intriguingly, recent experiments by Knops et al.[13] showed that the capillary breakup for multiple neighboring threads can occur simultaneously. Depending on the diameter of the threads, the distance between neighboring threads, and the thread-to-matrix viscosity ratio, these threads can break up via an "in-phase" or "out-of-phase" fashion.

Recently, we discovered that polystyrene (PS) threads (or stripes) cast on top of topographic poly(methyl methacrylate) (PMMA) patterns also showed simultaneous capillary breakup, creating a unique hierarchical composite film.[14,15] Here we present a systematic investigation of the influences of molecular weight and the as-cast volume of the PS on the morphological evolution of the PS/PMMA patterns upon thermal annealing. With proper control of these two factors, three regimes of phase evolution were observed: (1) a two-stage capillary breakup for low molecular weight and relatively small volume fraction of PS; (2) dewetting of PS on PMMA via random nucleation and growth for relatively thicker PS films with low molecular weight; (3) controlled nucleation of PS on PMMA mesas followed by capillary instability. Each type of phase

Received: December 14, 2011
Revised: January 26, 2012
Published: February 15, 2012

evolution resulted in a distinctive morphology featuring unique micro- and nanostructures.

2. EXPERIMENTAL SECTION

2.1. Materials. Monodisperse (PDI < 1.1) PMMA and PS were purchased from Polymer Source, Inc. and Scientific Polymer Products, Inc. All polymers were used as received, and their molecular weight and glass-transition temperature T_g are listed in Table 1. The T_gs of PS were estimated from literature.[16] As a confirmation of the reproducibility of the literature values, we sampled the T_gs of PS13k and PMMA12k for determination using the second Differential Scanning Calorimetry (NETZSCH DSC 204F1) scan at a heating rate of 20 °C/min.

Table 1. Molecular Weight and T_g of the Polymers Used in This Study

polymer	M_w (g/mol)	T_g (°C)	acronym
PMMA	12 000	107	PMMA12k
PS	4000	74[a]	PS4k
	13 000	87	PS13k
	31 600	97[a]	PS31.6k
	214 000	100[a]	PS214k
	2 000 000	100[a]	PS2000k

[a]Values obtained from ref 16.

2.2. Pattern Fabrication. PMMA thin films were first prepared by spin-coating toluene solutions containing 2.5 wt % of PMMA onto 0.38 mm thick silicon substrates that had previously been cleaned with piranha solution. The resulting PMMA films were subsequently annealed in a vacuum oven at 150 °C for 3 hours to remove the residual solvent. The initial thicknesses of the planar as-spincast PMMA films were determined to be ~150 nm. Surface grating patterns were fabricated onto the PMMA films via thermal embossing nanoimprint lithography (TE-NIL). The NIL process was performed on a nanoimprinter Eitrie 3 (Obducat Inc.) at 130 °C under a pressure of 4 MPa for 3 min. The same silicon mold was applied to all PMMA films in order to fabricate identical grating patterns with a pitch of 834 nm, a line-to-space ratio of 1, and a pattern height of 200 nm. AFM measurements of the as-imprinted PMMA patterns confirmed faithful replication of the mold pattern on all samples. Prior to the NIL, a self-assembled monolayer of tridecafluoro-1,1,2,2-tetrahydrooctyltrichlorosilane (Sigma-Aldrich, Inc.) was deposited on the surface of the mold through a vapor deposition process.[17] This effectively reduced adhesion between the mold and imprinted PMMA films, thus facilitating mold release at 70 °C (i.e., after PMMA was vitrified).

The PMMA used in this study had a molecular weight sufficiently below its critical molecular weight for entanglement ($M_c \approx 28$ kg/mol for bulk PMMA).[18,19] The patterned PMMA films were allowed adequate time for the residual stresses imposed by the NIL process to relax.[20,21] Subsequently, PS films were spin-cast onto the patterned PMMA films from 1-chloropentane (a selective solvent for PS[22]) solutions, with different weight fractions as specified in the discussion below, in order to obtain different thicknesses of the upper PS layer. The resulting PS/PMMA patterns were annealed at 60 °C (below the T_gs of both PS and PMMA) for 3 hours in vacuum to remove the residual solvents.

2.3. Characterization of Morphological Evolution upon Annealing. The PS/PMMA patterns were annealed under ambient conditions for different amounts of time, on a custom-made hot stage that had been calibrated with 7 melting-point standards (Sigma-Aldrich, Inc.) prior to use. The evolution of the surface morphology due to annealing was investigated with a Nikon LV150 optical microscope and a Dimension 3100 atomic force microscope (AFM). Furthermore, after selective removal of the top PS layer with cyclohexane, a selective solvent for PS,[23,24] we characterized the exposed PS/PMMA interface with AFM. All the AFM measurements were conducted using tapping mode with silicon cantilever probes that

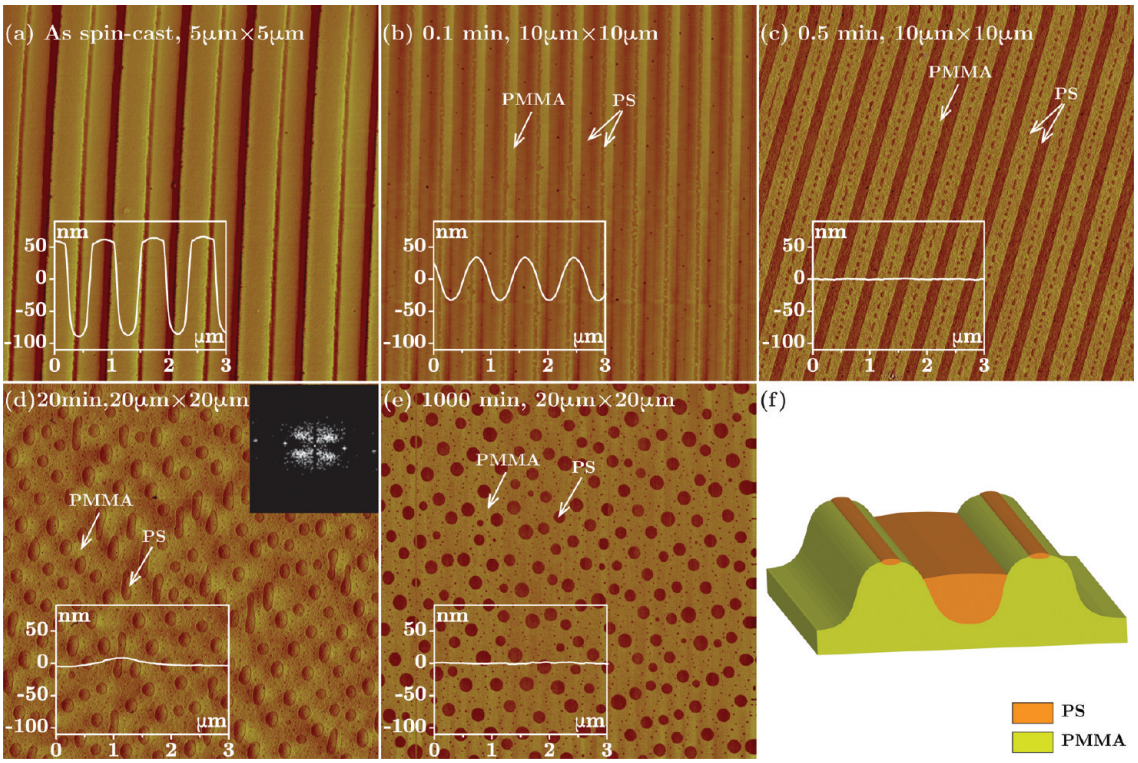

Figure 1. (a–e) AFM phase images of the PS214k/PMMA12k sample after annealing at 140 °C for different amounts of time, as labeled on each image. The insets are the representative cross-sectional profiles of each sample surface. (f) A schematic of the cross-section in part b.

dx.doi.org/10.1021/ma2026836 | Macromolecules 2012, 45, 1972–1981

have an estimated resonant frequency of 300 kHz and spring constants ranged from 25 to 75 N/m.

3. RESULTS AND DISCUSSION

3.1. Capillary Instabilities of PS Threads on PMMA Patterns.

3.1.1. Morphological Evolution. Recently, we reported the simultaneous breakup of PS13k threads that had been partially confined on PMMA12k patterns, when annealed at temperatures above the T_g of both polymers.[14] Here we first examine the generality of this capillary instability by varying the molecular weight of PS, ranged from 4 kg/mol to 2000 kg/mol, on identical PMMA12k substrates. For PS with molecular weight of 4 kg/mol up to 214 kg/mol, a type of two-step capillary instability was observed when the initial volume of PS cast on top of the PMMA pattern did not form a thick continuous layer, similar to what had been observed in the PS13k/PMMA12k.[14]

Figure 1 represents the distinctive stages during the morphological evolution in PS214k/PMMA12k. As detailed in the Experimental Section, the nanoimprinted PMMA pattern had a pattern height of 200 nm (see supplementary Figure S5, Supporting Information). After PS214k was cast onto the PMMA pattern, the average apparent pattern height became 143 nm, with PS distributed both on top of the mesas and within the trenches of the PMMA pattern. According to the mass conservation method described in our previous study,[14] we estimated the average thickness of PS214k on the mesas and trenches to be 12 and 63 nm, respectively. Just after 0.1 min of annealing at 140 °C, a temperature above the T_g of both polymers, the overall pattern height decreased to 67 nm (inset of Figure 1b), driven by the reduction of the overall polymer-surface energy. During this period, the PS on the PMMA mesas quickly retreated to the mesa centers, forming isolated narrow threads, while the PS in the trenches formed larger threads therein, as marked in Figure 1b, and schematically shown in Figure 1f.

After annealing for 0.5 min, the surface of the PS214k/PMMA system was completely smoothed out to minimize the polymer-surface area, resulting in a root mean square (RMS) surface roughness of $R_q \approx 0.49$ nm (see the inset of Figure 1c). During this period, the narrow PS threads on top of the PMMA mesas broke up into lines of droplets, driven by capillary instability seeking to minimize the total system energy (Figure 1c). Meanwhile, the width of the PS threads confined in the PMMA trenches shrank noticeably from 417 nm in the as-cast sample to ~300 nm. The mass transport associated with these subtle morphological changes was induced by the balance between the surface tension of the PS and the interfacial tension between the PS and PMMA, as discussed in the following section.

This intriguing surface pattern was preserved up to 10 min. Upon further annealing, the remaining larger PS threads also broke up into lines of droplets due to capillary instability. The characteristic wavelength of this capillary instability was determined to be 2.33 μm, from power spectrum density (PSD) analyses of the AFM phase images along the grating lines, after the threads completely broke up. As revealed in the FFT image (inset of Figure 1d), neighboring PS threads broke up simultaneously via an out-of-phase fashion, consistent with our previous report.[14] The sequential breakup of the two sets of PS threads led to a unique type of composite thin film: highly correlated PS214k droplets with a bimodal distribution in diameter (~600 nm for the larger droplets, ~65 nm for the smaller ones), all of which were partially embedded in the PMMA matrix. Upon further annealing, the morphological evolution was dominated by the coalescence among these PS droplets, reducing the PS/PMMA interfacial energy. Note that the overall surface of the film remained flat after the capillary breakup (cross-sectional profiles are shown in the insets of Figure 1d and e) and no dewetting of the PMMA matrix film was observed, since the SiO_x surface was wettable for the PMMA.

The aforementioned morphological evolution was observed for PS with molecular weights from 4 kg/mol to 214 kg/mol, as long as the as-cast PS on top of the PMMA pattern did not form a continuous thick layer (which will be discussed in section 3.2). Regardless, for these nonaxisymmetric PS threads that are partially embedded in the viscous PMMA matrix, there exists no theoretical model to describe the characteristic wavelength of the capillary instability and the corresponding breakup kinetics. In the following section, a static analysis of this system is presented first, and then experimental findings of the dependence of both the characteristic wavelength and breakup time on the viscosity ratio of the PS/PMMA are presented in section 3.1.3.

3.1.2. Static Analysis on the Capillary Instability of Nonaxisymmetric PS Threads. An axisymmetric liquid cylinder, with a radius r, completely embedded in an infinite immiscible viscous matrix breaks up into droplets due to Plateau–Rayleigh instability.[25,26] This is known to be caused by thermally induced surface fluctuations comprised of a rich spectrum of sinusoidal waves. As a sinusoidal fluctuation with a wavelength λ and amplitude α develops on the surface, conservation of the cylinder volume leads to a decrease in the average radius

$$r'^2 = r^2 - \alpha^2/2. \tag{1}$$

The total interfacial energy, E, of such a cylinder with a sinusoidal profile along the surface is[27]

$$E = 2\pi r'\lambda\gamma\left[1 + \left(\frac{\alpha\pi}{\lambda}\right)^2\right] \tag{2}$$

where γ is the interfacial tension between the thread and the matrix. From eq 1 and eq 2, it is clear that at the small perturbation limit, $\alpha\pi \ll \lambda$, E decreases with increasing fluctuating amplitude only for modes with wavelengths $\lambda > 2\pi r$.[28] Fluctuating waves with $\lambda < 2\pi r$ gradually damp out as they are energetically unfavorable.

In the following, we use a geometric analysis to determine the cutoff wavelength for the capillary instability of nonaxisymmetric liquid threads that are partially embedded in another viscous medium. Such threads were found at two different stages during annealing for our PS/PMMA system, for example, in the PS214k/PMMA12k system shown in Figure 1: ~80 nm wide PS threads on PMMA mesas as marked in Figure 1b, and ~300 nm wide PS threads originated from the PS cast into the PMMA trenches, as marked in Figure 1c. These PS threads were bounded by two interfaces, one air and the other PMMA. Since the cross-sectional length scale was well below the capillary length ($\kappa^{-1} = (\gamma/\rho g)^{1/2} \approx 1.8$ mm) of the PS at 140 °C, gravity was negligible compared to the surface/interfacial tension. The equilibrated cross sections of the two sets of PS threads, on mesas and within trenches, were similar in shape but different in size. In the following, we focus the

dx.doi.org/10.1021/ma2026836 | Macromolecules 2012, 45, 1972–1981

discussion on the larger PS threads confined within the PMMA trenches, because of the smaller experimental uncertainty.

As schematically shown in Figure 2, the cross-sectional shapes of the threads are determined by the balance of the

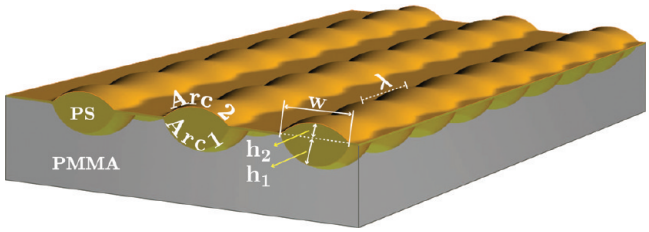

Figure 2. Schematic illustration of the sinusoidal fluctuations along the nonaxisymmetric PS threads that are partially embedded in the PMMA matrix. The geometry of the thread cross-section is marked (not actual size).

Laplace pressure at the PS−air surface with that at the PS/PMMA interface

$$\Delta P_{\text{Laplace}} = \frac{2\gamma_{S-M}}{r_1} = \frac{2\gamma_{PS}}{r_2} \tag{3}$$

where γ_{PS} and γ_{S-M} are the surface tension of the PS and the interfacial tension of the PS/PMMA, respectively. At a given annealing temperature, $\gamma_{PS} \gg \gamma_{S-M}$. For example, at 140 °C, γ_{PS} = 32.1 mN·m^{-1} (invariant in the range of PS molecular weights studied here) and γ_{S-M} = 1.6 mN·m^{-1}.[29] Therefore, the curvature of the PS/PMMA interface, Arc 1 (labeled in Figure 2), is significantly larger than that of the PS surface, Arc 2. Specifically, the radii of curvature of both arcs can be determined by

$$r_1 = \frac{w^2}{8h_1} + \frac{h_1}{2} \tag{4}$$

$$r_2 = \frac{w^2}{8h_2} + \frac{h_2}{2} \tag{5}$$

where the geometric parameters, w and h_1 can be determined by AFM measurements after selective removal of the PS. The corresponding central angles of both arcs are

$$\theta_1 = 2\arcsin\left(\frac{w}{2r_1}\right) \tag{6}$$

$$\theta_2 = 2\arcsin\left(\frac{w}{2r_2}\right) \tag{7}$$

When a thermally excited sinusoidal fluctuation with amplitude α and wavelength λ grows at the PS/PMMA interface, we assume that the corresponding fluctuation on the PS surface has the same wavelength but a much smaller amplitude $\alpha\gamma_{S-M}/\gamma_{PS}$, which is consistent with the observations from the AFM image (Figure 1c). At the small fluctuation limit, we derive the total surface/interfacial energy per unit length as

$$E(\alpha, \lambda) = \lambda\left\{\theta_1 r'_1\gamma_{S-M}\left[1 + \left(\frac{\alpha\pi}{\lambda}\right)^2\right] + \theta_2 r'_2\gamma_{PS}\left[1 + \frac{\left(\frac{\gamma_{S-M}}{\gamma_{PS}}\alpha\right)^2\pi^2}{\lambda^2}\right]\right\} \tag{8}$$

where the radii decreased according to eq 1. Unstable waves lead to reduction in E, which requires the first and second partial derivative of E, with respect to α at 0, should be zero and less than zero, respectively.[27] Taking the derivatives, we arrive at

$$\left.\frac{\partial E}{\partial \alpha}\right|_{\alpha=0} = 0 \tag{9}$$

$$\left.\frac{\partial^2 E}{\partial \alpha^2}\right|_{\alpha=0} = \frac{\gamma_{S-M}}{2\lambda}\left[\left(4\pi^2 r_1\theta_1 - \lambda^2\frac{\theta_1}{r_1}\right) + \left(4\pi^2\frac{\gamma_{S-M}}{\gamma_{PS}}r_2\theta_2 - \lambda^2\frac{\gamma_{S-M}\theta_2}{\gamma_{PS}r_2}\right)\right] < 0 \tag{10}$$

Equation 9 and 10 are necessary conditions for unstable waves to grow and lead to reduction in E. Equation 9 is ubiquitously satisfied and eq 10 yields only one legitimate inequality.

$$\lambda > 2\pi\sqrt{\frac{r_1\theta_1 + \frac{\gamma_{S-M}}{\gamma_{PS}}r_2\theta_2}{\frac{\theta_1}{r_1} + \frac{\gamma_{S-M}\theta_2}{\gamma_{PS}r_2}}} = 2\pi\sqrt{\frac{r_1(\theta_1 + \theta_2)}{\frac{\theta_1}{r_1} + \left(\frac{\gamma_{S-M}}{\gamma_{PS}}\right)^2\frac{\theta_2}{r_1}}} \tag{11}$$

Since $\theta_2 \ll \theta_1$ and $\gamma_{S-M} \ll \gamma_{PS}$, the inequality above can be simplified as

$$\lambda > 2\pi r_1 \tag{12}$$

i.e., only the initial radius of curvature at the PS/PMMA interface (Arc 1) is important for determining the cutoff wavelength, λ_c, above which the sinusoidal fluctuations on the strongly nonaxisymmetric liquid threads lead to a decrease of total system energy. In contrast, the PS−air surface plays only a minor role. Thus, the expression of λ_c for our nonaxisymmetric threads is the same as Plateau−Rayleigh's static analysis for an infinite perfect cylinder with identical radius r_1. By eq 11, we can estimate λ_c, for instance, in our PS31.6k/PMMA12k system, w = 400 nm, and h_1 = 140 nm. Solving eqs 3−7 gives the geometric parameters, r_1 = 212.0 nm, r_2 = 4150 nm, θ_1 = 2.47 rad, θ_2 = 0.096 rad. Plugging them in eq 11 gives λ_c for the nonaxisymmetric PS threads half-embedded in PMMA, $\lambda_c \approx$ 1.36 μm. From the experimental results shown below, the

dx.doi.org/10.1021/ma2026836 | Macromolecules 2012, 45, 1972−1981

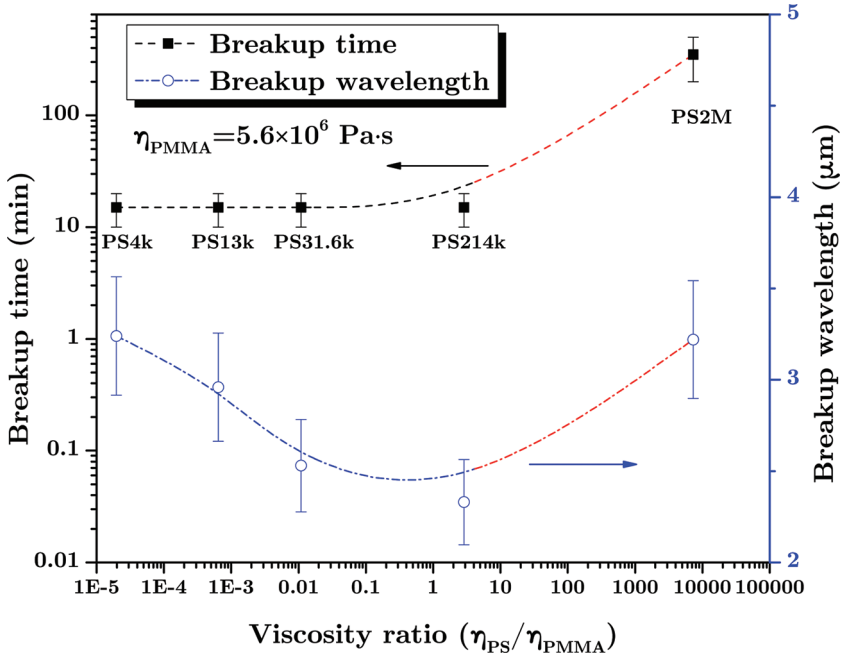

Figure 3. Influence of thread-to-matrix viscosity ratio on both the breakup time and characteristic wavelength of the capillary instability for the PS threads confined in the PMMA trenches after annealing at 140 °C. The dashed lines are a guide to the eye only.

minimum wavelength for the unstable capillary fluctuations for the partially embedded PS threads is indeed determined by the radius of curvature of the liquid−liquid interface r_1.

For our nonaxisymmetric threads, the following has to be taken into consideration additionally: (a) the different curvatures on the PS−air and the PS−PMMA side; (b) the difference between PS−air surface tension and PS−PMMA interfacial tension, and (c) the different viscosities of PMMA and air. An exact analytic or numeric treatment is still lacking in literature.

3.1.3. Characteristic Wavelength and Breakup Time of These Nonaxisymmetric PS Threads. As discussed above, all sinusoidal fluctuations with wavelengths above λ_c would lead to a reduction in the surface/interfacial energy of the system. However, oftentimes the morphology of the capillary breakup observed does not reflect such a broad distribution in wavelengths (Figure 1e). Rather, it reveals a characteristic/dominant wavelength. For an axisymmetric thread embedded in an immiscible viscous fluid matrix, Tomotika's pioneering theoretical work shows that the unstable sinusoidal fluctuations grow at significantly different rates.[12] The fastest growing mode quickly eclipses others and dominates the final morphology. Both the wavelength and the growth rate of the dominant mode is a known function of the initial cylinder radius and thread-to-matrix viscosity ratio.[12]

Here we provide first-hand experimental findings of both the characteristic wavelength and the breakup time of these nonaxisymmetric PS threads with varying molecular weights. As detailed in the Experimental Section, PS with molecular weight ranged from 4 kg/mol to 2000 kg/mol was examined while PMMA was kept identical, which allows for the thread-to-matrix viscosity ratio to span 10 orders of magnitude. Each sample was annealed at 140 °C, similar to the sample shown in Figure 1, and the evolving morphologies were determined with AFM. Similar to the PS214k/PMMA system discussed above, the characteristic wavelength for the capillary instability in each sample was determined from the PSD analysis of the AFM images. Furthermore, the breakup time, defined as the time at which the isolated droplets were formed, was obtained from the AFM measurements for each sample.

Figure 3 plots both the characteristic wavelength and the breakup time as a function of the thread-to-matrix viscosity ratio for all the samples studied. Here, the steady-state viscosity for both the monodisperse PS and PMMA were estimated from Majeste et al.[30] and Ahn et al.,[15] correspondingly. As shown in Figure 3, viscosities of the PS threads are significantly lower than that of the PMMA matrix for PS molecular weights smaller than 214 kg/mol, and become comparable to the matrix viscosity at 214 kg/mol. In this regime, the breakup time remains rather constant (~20 min) even though the thread-to-matrix viscosity ratio has increased 10 000 times, indicating that the breakup time is dictated by the invariant viscosity of the PMMA matrix. In contrast, as the PS molecular weight increases from 214 kg/mol to 2000 kg/mol, the thread viscosity becomes significantly larger than that of the PMMA matrix, and the breakup time increases dramatically from ~20 min to ~500 min. This suggests that the viscosity of the PS threads dictates the breakup kinetics.

From Figure 3, it is apparent that the more viscous component, either the threads or the matrix, is the rate-limiting factor for the breakup of the threads. Although a rigorous theoretical account of the kinetics of the capillary breakup of a nonaxisymmetric thread is still lacking, the qualitative trend is consistent with the two limiting cases in Tomotika's theory. Specifically, the growth rate, *in*, for an axisymmetric PS thread

dx.doi.org/10.1021/ma2026836 | *Macromolecules* 2012, 45, 1972−1981

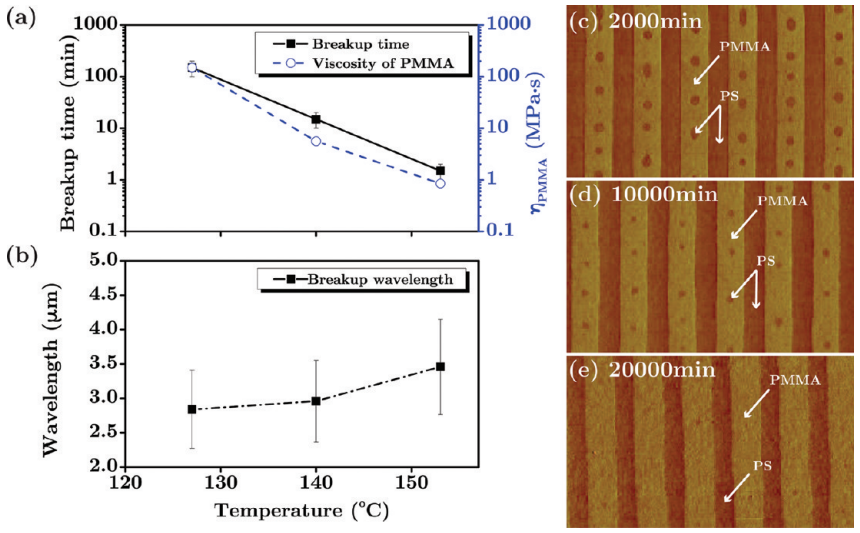

Figure 4. Influence of annealing temperature on (a) the time scale and viscosity of PMMA for the PS13k/PMMA12k system and (b) the characteristic wavelength of the capillary breakup. (c–e) AFM phase images (5 μm × 3 μm) of the sample surface after annealing at 114 °C for different amounts of time as labeled. The bright and dark regions correspond to the PMMA and PS domains, respectively.

completely embedded in a PMMA matrix, at the two extremes of viscosity ratios are

$$in = \begin{cases} \dfrac{1}{\eta_{PMMA}} \dfrac{\gamma_{S-M}\Omega_1(kr)}{2r}, & \eta_{PS}/\eta_{PMMA} \to 0 \\ \dfrac{1}{\eta_{PS}} \dfrac{\gamma_{S-M}\Omega_2(kr)}{2r}, & \eta_{PS}/\eta_{PMMA} \to \infty \end{cases} \tag{13}$$

where k is the wavenumber and r is the initial radius of the thread. $\Omega_1(kr)$ and $\Omega_2(kr)$ are nondimensional single-variable functions of kr, characterizing the growth rate of a perturbation with wavenumber k. Therefore, the more viscous component, thread or matrix, will dominate the growth rate or the breakup time of the threads, indicated by the viscosity terms in the denominators.

Since the viscosity of air is negligible compared to the polymers, the breakup kinetics is dictated by the PS/PMMA interface. This is also manifested by the morphology or the characteristic wavelength of the fastest growing mode. As shown in Figure 3, the characteristic wavelengths for all samples were around 3 μm, all of which were above the cutoff wavelength of each respective sample (~1.36 μm). The cutoff wavelength did vary slightly with the amount of PS cast. The error bars in the breakup time represent the upper and lower bound limited by experimental resolution, while for the breakup wavelength, they represent 10% off-peak values in our PSD fitting analysis. Interestingly, it appears that the breakup wavelength reaches a minimum when the thread-to-matrix viscosity ratio approaches 1. A calculation based on Tomotika's classical theory by Knops et al.[13] shows that, for a completely embedded axisymmetric viscous thread, the breakup wavenumber (inverse of breakup wavelength) reaches maximum at a thread-to-matrix viscosity ratio near 1 (see Figure 1 from ref 13). Although the exact physical system and geometries in our experiments were different from ref 13, the similarity indicates again the PS/PMMA interface plays a dominating role in choosing the fastest mode. On the other hand, if the PS/air surface was dominant, the fastest growing wavelength of a PS thread in air would tend to infinity,[12] disagreeing with the experimental results. As noted above, a rigorous theoretical work is still needed to describe both the wavelength and the growth rate associated with the fastest growing mode for a partially embedded nonaxisymmetric thread.

3.1.4. Influence of Annealing Temperature on the Capillary Instability of PS13k/PMMA12k. As discussed above, in the low thread-to-matrix viscosity ratio regime, the breakup time is controlled by the PMMA matrix viscosity. To further verify this, we annealed the samples at different temperatures. PS13k/PMMA12k system was annealed at 114, 127, 140, and 153 °C. At the three higher temperatures, the morphological evolutions, according to the AFM measurements, were similar to that shown in Figure 1.

The breakup time and characteristic wavelength of the capillary instability (for the larger PS threads confined in the PMMA trenches) are shown in Figure 4, parts a and b. Clearly, with the increase of annealing temperature, the breakup time was reduced dramatically while the breakup wavelength remained ~3 μm. It is known that PS and PMMA are "fragile" glass-forming liquids, whose viscosities have a similar dependence on temperatures.[31] Therefore, the viscosity ratio is not expected to vary significantly with the increase of annealing temperature, while the absolute values of the viscosities of both polymers decrease dramatically. Since reducing the PS viscosity over 5 orders of magnitude while keeping the matrix viscosity constant did not affect the breakup time, the significant reduction in breakup time with the increase of annealing temperature was most likely caused by the dramatic reduction in the matrix viscosity. In particular, Figure 4 shows 2 orders of magnitude of reduction in the viscosity of PMMA matrix, similar to the change observed in the breakup time.

The morphological evolution became extremely slow at 114 °C, a temperature slightly above the bulk T_g of PMMA (107 °C). Figure 4c–e show that the isolated larger PS threads remained unbroken even after 20000 min of annealing, once again suggesting that the PMMA viscosity dominated the breakup time of the PS threads. In comparison, the smaller PS threads (or stripes) on top of the PMMA mesas had completely broken up into droplets after 2000 min annealing. A similar

dx.doi.org/10.1021/ma2026836 | Macromolecules 2012, 45, 1972–1981

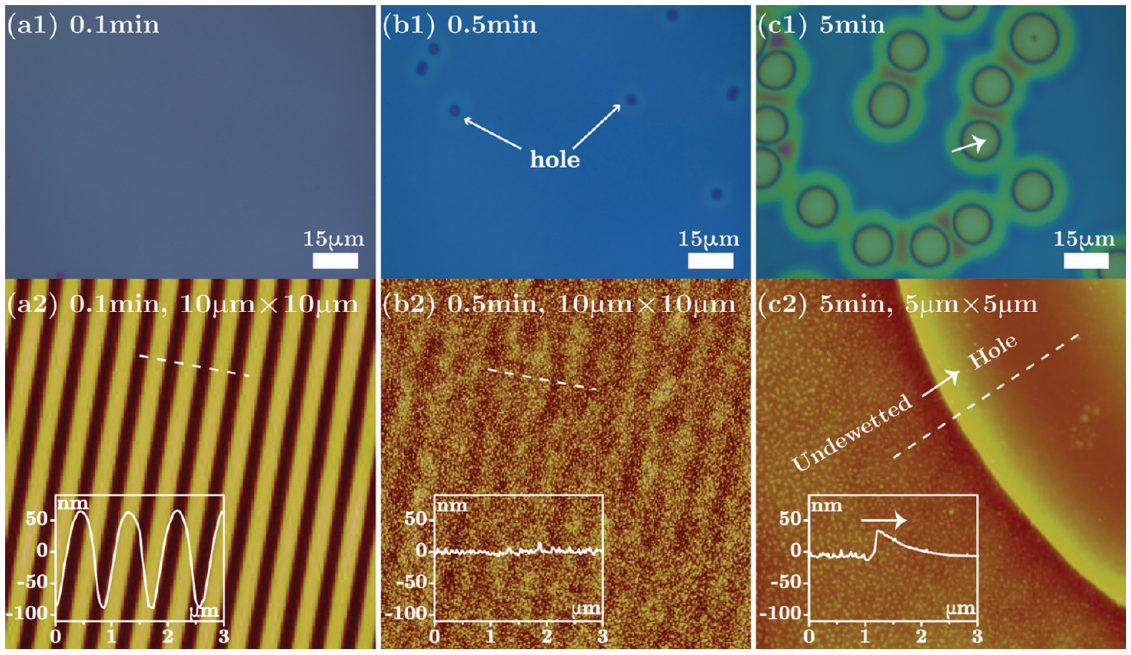

Figure 5. Morphologies of a thick PS layer, cast from 1.8 wt % solution, on the PMMA pattern, upon annealing at 153 °C for different amounts of time as labeled on the images. (a1−c1) Optical images of the sample surface. (a2−c2) Corresponding topographic AFM images of the PS/PMMA interface after selective removal of PS with cyclohexane. Insets in parts a2−c2 are the cross-sectional profiles.

trend was also observed for the partially embedded PS threads (Figure 1). In addition to the geometric reasons, it might also be that the effective viscosity of the PS within the ultrathin threads on the mesas (less than 20 nm, determined after selectively dissolve the PS) is much smaller than that of the larger ones. This could possibly be resultant from confinement-induced T_g reduction.[32] Interestingly, during extended annealing, the isolated PS droplets (radius ≈ (90−100) nm, depth ≈ (60−70) nm), gradually "sank" into the underlying PMMA, presumably to reduce the total surface/interfacial energy.

In contrast to the significant dependence of kinetics on the temperature, few variations in the breakup wavelength were found at the three annealing temperatures (Figure 4a). As discussed above, since the thread-to-viscosity ratio remained rather constant at different annealing temperatures and the geometry and boundary conditions were identical, the breakup wavelength was expected to be similar, as observed in Figure 4a.

3.2. Influence of the PS Film Thickness on the Instability of the PS/PMMA Patterns. The two-stage capillary instability discussed above was observed for all the systems, in which PS top layer did not form a thick continuous layer after short annealing. In order to draw a complete picture regarding the role of the PS film thickness, both PS13k and PS2000k films were cast onto the PMMA12k pattern from toluene solutions with varying concentrations. Their corresponding morphological evolutions upon thermal annealing are discussed below.

3.2.1. PS13k/PMMA12k. The deposition of PS onto topographically patterned surfaces via spin-coating is influenced by the interplay between flow and evaporation.[33,34] The spin-coating process of polymer solutions consists of two stages, flow-dominant stage and evaporation-dominant stage. Studies show that a critical film thickness divides the two stages. In the second stage, the fluid becomes so viscous that it ceases to flow.[33] After reaching this critical thickness, evaporation of the solvent dictates the partitioning of the PS. Qualitatively, when using higher concentrations of PS solutions, the critical thickness should be reached quicker,[35] leaving more PS deposited on the PMMA patterns. When the PS13k solution concentration was 0.5 and 1.0 wt %, the as-cast PS did not form a continuous layer. As a result, a similar two-stage capillary breakup was observed (similar to that in Figure 1) with slight differences in the breakup time and wavelength that were caused by the differences in the width (or the amount) of the PS threads. As expected, the PS droplets formed from the use of the 1.0 wt % solution were larger than those formed when using the 0.5 wt % solution (see Figure S1, Supporting Information).

In contrast, for PS cast from 1.8 and 2.5 wt % solutions, no capillary instability was observed. For example, for PS cast from 1.8 wt % solution, both the PS surface and PS/PMMA interface (Figure 5a1 and a2) smoothed out quickly upon annealing and reached a planar bilayer configuration (Figure 5b1 and b2). AFM images of the PS/PMMA interface pattern heights became as small as few nanometers (Figure 5b2), and circular holes were nucleated within the PS film (Figure 5b1). The growth of these holes eventually led to the complete dewetting of the PS, forming PS droplets on top of the PMMA (not shown). This nucleation and growth mechanism is similar to that of a 65 nm thick PS13k film on top of a viscous PMMA substrate.[14] Furthermore, the AFM measurements revealed a characteristic undercut profile (inset of Figure 5c2) after selectively removing the top PS layer. This type of interfacial profile at the dewetting rim in Figure 5c1 is consistent with that observed in the dewetting of PS planar film on top of a viscous PMMA film (regime I in ref 24).

3.2.2. PS2000k/PMMA12k Patterns. Both the capillary instability and dewetting described above are characteristic viscous instabilities driven by the minimization of surface/interfacial energy of the system via viscous dissipation. With an increase in molecular weight, the viscoelasticity of the polymers

dx.doi.org/10.1021/ma2026836 | *Macromolecules* 2012, 45, 1972−1981

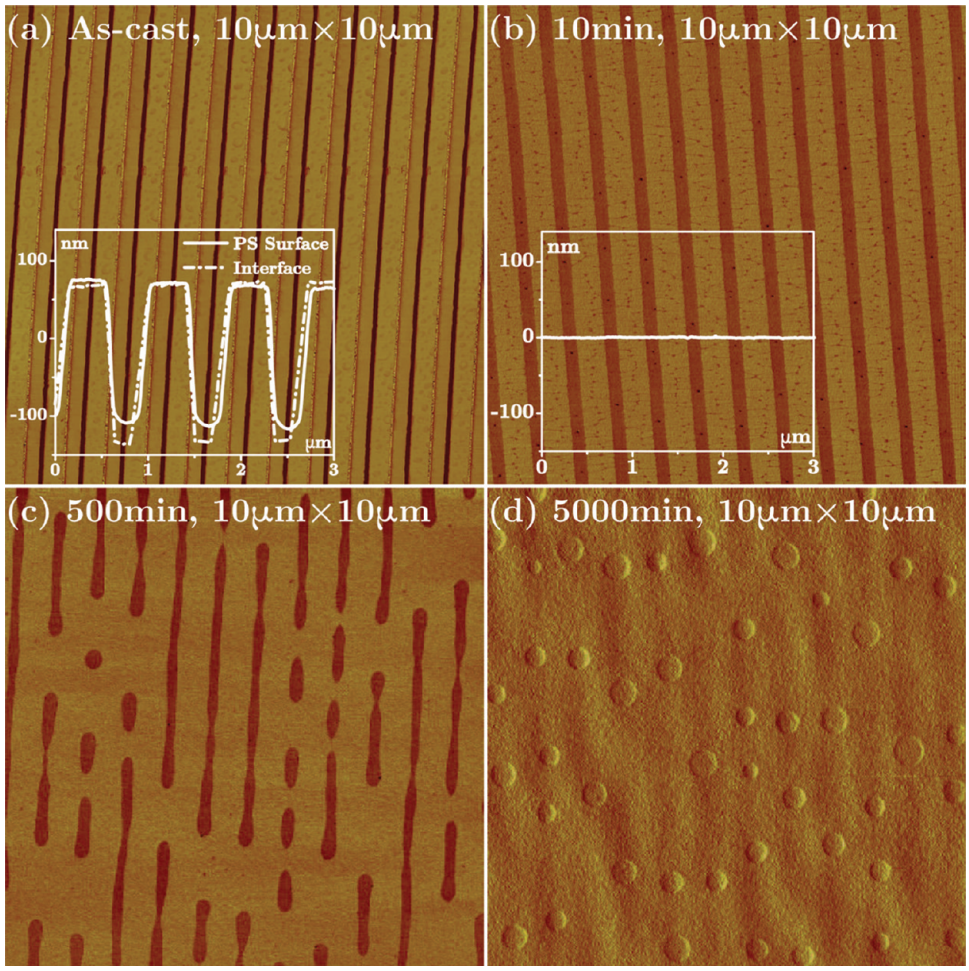

Figure 6. AFM phase images of PS2000k (cast from 0.6 wt % solution)/PMMA12k patterns after annealing at 140 °C for different amounts of time as labeled on the images. The inset in part a shows the representative cross-sectional profiles of both the PS surface and PS−PMMA interface. The inset in part b shows the cross-sectional profile of the surface.

becomes increasingly evident. Here, PS2000k films with varying thickness were cast onto the PMMA12k patterns, from toluene solutions with concentrations of 0.6, 0.8, and 1.0 wt %, to examine the influence of the viscoelasticity on the overall film instabilities.

Figure 6 shows that the morphological evolution in PS2000k0.6%/PMMA was similar to the one shown in Figure 1: a quick surface leveling led to isolated PS stripes/threads, which broke up via capillary instability. Because of the low concentration of PS solution used, the PS stripes left on top of the PMMA mesas were only around 3 nm thick (inset of Figure 6a), which did not show a clear capillary breakup. The capillary breakup of the larger threads confined in PMMA trenches (~23 nm thick after casting) shows that the breakup time (~500 min) was significantly longer than that of the lower molecular weight PS (~20 min) at the same annealing temperature, as shown in Figure 3.

In comparison, PS2000k cast from 0.8 and 1.0 wt % solution onto the PMMA pattern showed distinctive morphological evolutions, the latter of which is shown in Figure 7 (the images for PS2000k cast from 0.8% solution are provided in Figure S3, Supporting Information). The as-cast pattern has a cross-sectional profile showing round and smooth tops as opposed to the flat edged tops in PS2000k0.6%/PMMA system (Figure S2, Supporting Information). This curvature strongly suggests a continuous coverage of the PS2000k capping layer over the PMMA patterns. After 20 min, the surface of the PS decayed to ~6 nm tall (Figure 7a). The apexes of the PS lines were at the center of the PMMA trenches, while valleys corresponded to the PS on the PMMA mesas (Figure 7a).

After 50 min, holes were found to be nucleated in the PS upper layer on top of the PMMA mesas, where the PS film was the thinnest (Figure 7b). This time scale was significantly shorter than the capillary-breakup time for the isolated PS2000k threads in Figure 6. The growth/merging of these holes caused the PS threads to bend and form bridges between neighboring ones. The result was a mesh-like PS structures on top of the PMMA film after 100 min of annealing. The mesh-like structure in the PS2000k0.6%/PMMA system appears evidently different, in terms of diameter and connectivity, from PS2000k0.8%/PMMA system (Figure S3 in Supporting Information), which suggests concentration of spin-coating solution as a controlling parameter. This mesh-like network then evolved via local merging of PS threads, which eventually ruptured into isolated droplets via capillary instability after 1000 min (Figure 7, parts d and e). This rupture time was longer than that observed in Figure 6, because the average diameter/cross-section of the threads in the mesh-like structure was larger. Further annealing led to the shape changes of the isolated PS droplets driven by the interfacial tension (Figure

dx.doi.org/10.1021/ma2026836 | *Macromolecules* 2012, 45, 1972−1981

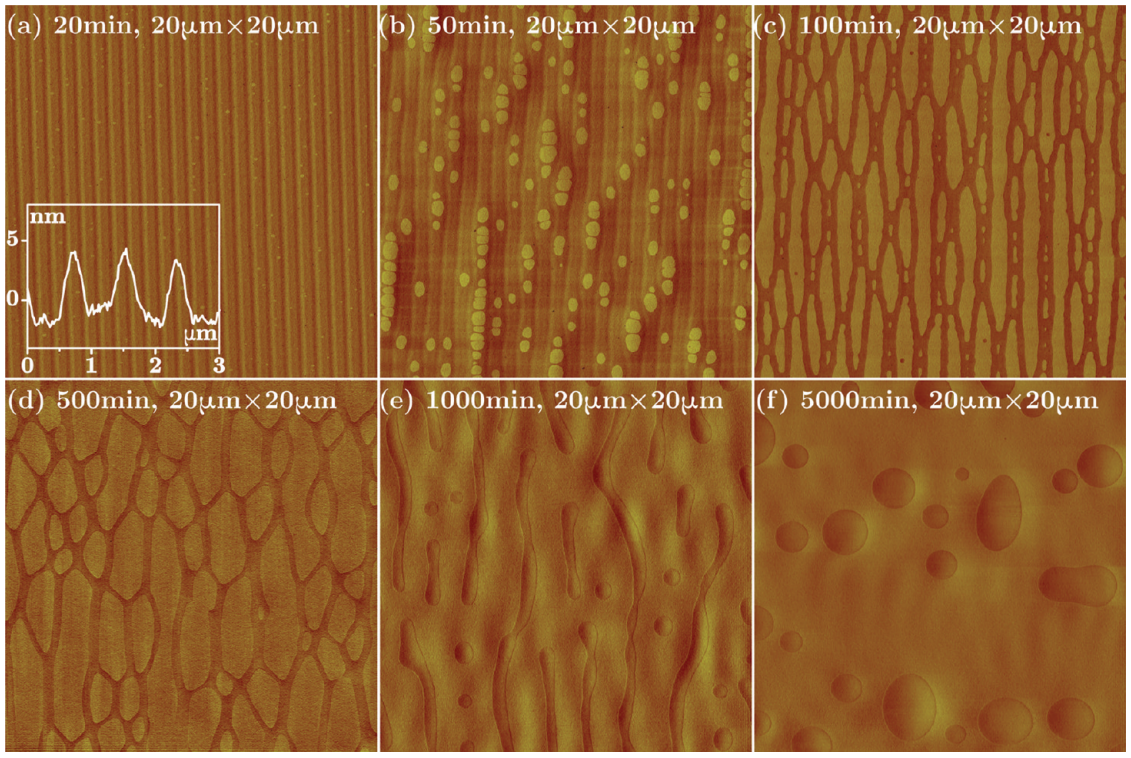

Figure 7. AFM phase images of PS2000k (cast from 1.0 wt % solution)/PMMA12k patterns after annealing at 140 °C for different amounts of time as labeled on the images. The inset in part a shows the cross-sectional profile of the sample surface for the corresponding sample.

7f). Clearly, the distribution of the diameter of the PS droplets is much broader than the one shown in Figure 6, due to the formation of the intermediate mesh-like morphology. Clearly, the elasticity of the highly entangled polymers, manifested in the bending of the lines, can signficantly influence the final morphology resulted from viscous instabilty.

4. CONCLUSIONS

In this study, we systematically examined the instability of the bilayer polymer patterns formed by casting of PS onto topographic PMMA patterns and subsequent thermal annealing at temperatures above the T_g of both polymers. A range of instabilities were observed depending on the molecular weight and amount of PS cast on the PMMA.

When the PS cast on the PMMA pattern did not form a continuous layer, a two-stage capillary instability was observed. Upon annealing, the PS quickly formed confined threads both on top of the PMMA mesas and within the PMMA trenches. These nonaxisymmetric PS threads, partially embedded in the PMMA matrix, broke up into isolated droplets via capillary instability. Systematic measurements showed that the breakup time depended on the thread-to-matrix viscosity and was dictated by the more viscous phase. In contrast, the characteristic wavelength of the capillary breakup only slightly depended on the viscosity ratio, and reached a minimum as the viscosity ratio approached 1. Although these experimental results can be qualitatively understood from the limiting cases of Tomotika's theory, an exact theoretical description of the capillary instability in such nonaxisymmetric threads is still lacking.

When the top PS layer was thick enough to form a continuous layer shortly after annealing, the instability of the film varied with the molecular weight of the PS. When the molecular weight of the PS was low, a planar PS/PMMA bilayer was formed after annealing. Subsequently, the PS upper layer dewetted from the PMMA via a random nucleation and growth mechanism. For high molecular weight PS, the PS/PMMA interface remained corrugated with a continuous PS layer on top. Localized nucleation in the PS layer occurred on top of the PMMA mesas, which resulted in a mesh-like PS morphology. Eventually, this PS fibrillar network broke into droplets due to capillary instability. Therefore, by controlling the molecular weight and spin-cast volume, a rich spectrum of micro- and nanoscale structures can be obtained that are potentially useful for a range of applications.

■ ASSOCIATED CONTENT

Supporting Information

AFM phase images, AFM height images, and a cross-sectional profile. This material is available free of charge via the Internet at http://pubs.acs.org/.

■ AUTHOR INFORMATION

Corresponding Author

*E-mail: Yifu.Ding@Colorado.edu.

Notes

The authors declare no competing financial interest.

■ ACKNOWLEDGMENTS

The authors acknowledge the funding support from the National Science Foundation under Grant No. CMMI-1031785. Acknowledgment is made to the donors of the Petroleum Research Fund, administered by the American Chemical Society, for partial support of this research (Grant Number: ACS-PRF 50581-DNI7).

REFERENCES

(1) Xie, R.; Karim, A.; Douglas, J. F.; Han, C. C.; Weiss, R. A. *Phys. Rev. Lett.* **1998**, *81*, 1251−1254.
(2) Schäffer, E.; Harkema, S.; Roerdink, M.; Blossey, R.; Steiner, U. *Macromolecules* **2003**, *36*, 1645−1655.
(3) Schäffer, E.; Thurn-Albrecht, T.; Russell, T. P.; Steiner, U. *Nature* **2000**, *403*, 874−877.
(4) Morariu, M. D.; Voicu, N. E.; Schäffer, E.; Lin, Z.; Russell, T. P.; Steiner, U. *Nat. Mater.* **2002**, *2*, 48−52.
(5) Reiter, G. *Phys. Rev. Lett.* **1992**, *68*, 75−78.
(6) Reiter, G. *Langmuir* **1993**, *9*, 1344−1351.
(7) Stange, T. G.; Evans, D. F.; Hendrickson, W. A. *Langmuir* **1997**, *13*, 4459−4465.
(8) Higgins, A. M.; Jones, R. A. L. *Nature* **2000**, *404*, 476−478.
(9) Herminghaus, S.; Brinkmann, M.; Seemann, R. *Annu. Rev. Mater. Res.* **2008**, *38*, 101−121.
(10) Rockford, L.; Liu, Y.; Mansky, P.; Russell, T. P.; Yoon, M.; Mochrie, S. G. J. *Phys. Rev. Lett.* **1999**, *82*, 2602−2605.
(11) Sehgal, A.; Ferreiro, V.; Douglas, J. F.; Amis, E. J.; Karim, A. *Langmuir* **2002**, *18*, 7041−7048.
(12) Tomotika, S. *Proc. R. Soc. London, Ser. A: Math. Phys. Sci.* **1935**, *150*, 322−337.
(13) Knops, Y. M. M.; Slot, J. J. M.; Elemans, P. H. M.; Bulters, M. J. H. *AIChE J.* **2001**, *47*, 1740−1745.
(14) Ahn, D. U.; Wang, Z.; Yang, R.; Ding, Y. *Soft Matter* **2010**, *6*, 4900−4907.
(15) Ahn, D. U.; Ding, Y. *Soft Matter* **2011**, *7*, 3794−3800.
(16) Ding, Y.; Kisliuk, A.; Sokolov, A. P. *Macromolecules* **2004**, *37*, 161−166.
(17) Jung, G.; Li, Z.; Wu, W.; Chen, Y.; Olynick, D. L.; Wang, S.; Tong, W. M.; Williams, R. S. *Langmuir* **2005**, *21*, 1158−1161.
(18) Ferry, J. *Viscoelastic properties of polymers*, 3rd ed.; Wiley: New York, 1980.
(19) Kumaraswamy, G.; Ranganathaiah, C. *Polym. Eng. Sci.* **2006**, *46*, 1231−1241.
(20) Ding, Y.; Ro, H.; Douglas, J.; Jones, R.; Hine, D.; Karim, A.; Soles, C. *Adv. Mater.* **2007**, *19*, 1377−1382.
(21) Ding, Y.; Ro, H. W.; Germer, T. A.; Douglas, J. F.; Okerberg, B. C.; Karim, A.; Soles, C. L. *ACS Nano* **2007**, *1*, 84−92.
(22) Ennis, D.; Betz, H.; Ade, H. *J. Polym. Sci., Part B: Polym. Phys.* **2006**, *44*, 3234−3244.
(23) Wang, C.; Krausch, G.; Geoghegan, M. *Langmuir* **2001**, *17*, 6269−6274.
(24) Lambooy, P.; Phelan, K. C.; Haugg, O.; Krausch, G. *Phys. Rev. Lett.* **1996**, *76*, 1110−1113.
(25) Rayleigh, L. *Philos. Mag.* **1892**, *34*, 145.
(26) Rayleigh, L. *Philos. Mag.* **1892**, *34*, 177.
(27) Son, Y.; Martys, N. S.; Hagedorn, J. G.; Migler, K. B. *Macromolecules* **2003**, *36*, 5825−5833.
(28) de Gennes, P.; Brochard-Wyart, F.; Quere, D. *Capillarity and wetting phenomena: drops, bubbles, pearls, waves*, 1st ed.; Springer: Berlin, 2003.
(29) Mark, J. E. *Physical Properties of Polymers Handbook*, 2nd ed.; Springer: New York, 2007.
(30) Majeste, J.; Montfort, J. P.; Allal, A.; Marin, G. *Rheol. Acta* **1998**, *37*, 486−499.
(31) Böhmer, R.; Ngai, K. L.; Angell, C. A.; Plazek, D. J. *J. Chem. Phys.* **1993**, *99*, 4201.
(32) Alcoutlabi, M.; McKenna, G. B. *J. Phys.: Condens. Matter* **2005**, *17*, R461−R524.
(33) Meyerhofer, D. *J. Appl. Phys.* **1978**, *49*, 3993.
(34) Yu, Z.; Hwu, J.; Liu, Y.; Gauzner, G.; Lee, K.; Kuo, D. *J. Appl. Phys.* **2011**, *110*, 014303.
(35) Hall, D. B.; Underhill, P.; Torkelson, J. M. *Polym. Eng. Sci.* **1998**, *38*, 2039−2045.